

Manuscript Number: CRST-D-15-00045

Title: Network Modeling of Arctic Melt Ponds

Article Type: Research Paper

Keywords: Melt ponds; Horizontal Conductivity; Mathematical Morphology; Graph Theory

Corresponding Author: Ms. Meenakshi Barjatia, M.S.

Corresponding Author's Institution: University of Utah

First Author: Meenakshi Barjatia, M.S.

Order of Authors: Meenakshi Barjatia, M.S.; Tolga Tasdizen, Ph.D.; Boya Song; Kenneth M Golden, Ph.D.

**Abstract:** The recent precipitous losses of summer Arctic sea ice have outpaced the projections of most climate models. Efforts to improve these models have focused in part on a more accurate accounting of sea ice albedo or reflectance. In late spring and summer, the albedo of the ice pack is determined primarily by melt ponds that form on the sea ice surface. The transition of pond configurations from isolated structures to interconnected networks is critical in allowing the lateral flow of melt water toward drainage features such as large brine channels, fractures, and seal holes, which can significantly alter the albedo. Moreover, pond connectivity can also influence their effectiveness in breaking up an ice floe as the melt season progresses. Here we develop algorithmic techniques for mapping photographic images of melt ponds onto discrete conductance networks which represent the geometry of pond configurations and approximate the ease of lateral flow. We implement an image processing algorithm with mathematical morphology operations to produce a conductance matrix representation of the melt ponds. Basic clustering and edge elimination using graph theory is then used to map the melt pond connections and reduce the conductance matrix to include only direct connections. The results for images taken during different times of the year are visually inspected and the number of mislabels is used to evaluate performance.

Meenakshi Barjatia  
Electrical and Computer Engineering  
University of Utah

16th Feb, 2015

Dear Dr. Sulsky,

This letter is regarding the submission of a manuscript titled 'Network Modeling of Arctic Melt-Ponds' to the 'Cold Regions Science and Technology' journal.

In this manuscript, we describe our method for generating network models for arctic melt ponds. Image processing techniques and graph theory are used to model interconnected networks of arctic melt ponds as nodes and edges. Conductance graphs are generated for melt pond networks. These conductance graphs may be related to horizontal fluid conductivity in melt pond networks and this needs to be further explored.

We hope that this manuscript will be suitable for publication in this journal.

Thank you for your consideration of this manuscript.

Sincerely,  
Meenakshi Barjatia

# Network Modeling of Arctic Melt Ponds

Meenakshi Barjatia<sup>a</sup>, Tolga Tasdizen<sup>a,b,\*</sup>, Boya Song<sup>c</sup>, Kenneth M. Golden<sup>c</sup>

<sup>a</sup>*Electrical and Computer Engineering, University of Utah*

<sup>b</sup>*Scientific Computing and Imaging Institute, University of Utah*

<sup>c</sup>*Department of Mathematics, University of Utah*

---

## Abstract

The recent precipitous losses of summer Arctic sea ice have outpaced the projections of most climate models. Efforts to improve these models have focused in part on a more accurate accounting of sea ice albedo or reflectance. In late spring and summer, the albedo of the ice pack is determined primarily by melt ponds that form on the sea ice surface. The transition of pond configurations from isolated structures to interconnected networks is critical in allowing the lateral flow of melt water toward drainage features such as large brine channels, fractures, and seal holes, which can significantly alter the albedo. Moreover, pond connectivity can also influence their effectiveness in breaking up an ice floe as the melt season progresses. Here we develop algorithmic techniques for mapping photographic images of melt ponds onto discrete conductance networks which represent the geometry of pond configurations and approximate the ease of lateral flow. We implement an image processing algorithm with mathematical morphology operations to produce a conductance matrix representation of the melt ponds. Basic clustering and edge elimination using graph theory is then used to reduce the conductance matrix to include only direct connections. The results for images taken during different times of the year are visually inspected and the number of mislabels is used to evaluate performance.

*Keywords:* Melt ponds, Horizontal Conductivity, Mathematical Morphology, Graph Theory

---

## 1. Introduction

Sea ice is a critical component of Earth's climate system, and a sensitive indicator of climate change. The dramatic losses of summer Arctic sea ice observed in the past few decades have a substantial impact on Earth's climate system, yet most global climate models have significantly underestimated the rate of decline [1, 2, 3]. One of the fundamental challenges of climate science is to develop more rigorous representations of sea ice in climate models, and incorporate important small scale processes and structures into these large scale models. For example, during the melt season the Arctic sea ice cover becomes a complex, evolving mosaic of ice, melt ponds on the sea ice surface, and open water. While white snow and ice reflect most incident sunlight, melt ponds and ocean absorb most of it. The overall reflectance or albedo of sea ice floes – the ratio of reflected to incident sunlight – is determined by the evolution of melt pond coverage and geometry [4, 5, 6]. As melting increases, the albedo is lowered, which increases solar absorption, leading to more

melting, and so on. This critical mechanism is called *ice-albedo feedback* [7], and has played a significant role in the decline of the summer Arctic ice pack [8]. Sea ice albedo is a significant source of uncertainty in climate projections and one of the most important parameters in climate modeling [9, 5, 10, 6].

While melt ponds form a key component of the Arctic marine environment, comprehensive observations or theories of their formation, coverage, and evolution remain relatively sparse. Available observations of melt ponds show that their areal coverage is highly variable, particularly for first year ice early in the melt season, with rates of change as high as 35% per day [11, 6]. Such variability, as well as the influence of many competing factors controlling melt pond and ice floe evolution, makes the incorporation of realistic treatments of albedo into climate models quite challenging [6]. Small and medium scale models of melt ponds which include some of these mechanisms have been developed [12, 13, 5], and melt pond parameterizations are being incorporated into global climate models [9, 14, 10].

As melting progresses during the season,

---

\*Corresponding author, email: tolga@sci.utah.edu, Ph:1-801-581-3539

the evolution of melt ponds from small isolated structures into large interconnected networks is responsible for a number of processes that help control the rate at which the ice pack melts. It is believed [15] that this evolution of connectedness is an example of a percolation transition [16, 17]. Such a transition occurs when one phase in the microstructure of a composite material, for example, becomes connected on macroscopic scales as some parameter exceeds a critical value, called the *percolation threshold* [16, 17]. Percolation theory was initiated in 1957 by Broadbent and Hammer- sly [18] with the introduction of a simple lattice network model to study the flow of air through permeable sandstones used in miner’s gas masks. In subsequent decades, this theory has been used to successfully model a broad array of disordered materials and processes. In the case of melt ponds, the critical threshold is thought to be related to the area fraction of sea ice surface covered by the ponds.

An important example of this percolation phenomenon in the microphysics of sea ice, which itself is fundamental to the process of melt pond drainage and changes in sea ice albedo, is the percolation transi-

tion exhibited by the brine phase in sea ice, known as the *rule of fives* [19, 20, 21]. When the brine volume fraction of columnar sea ice is below about 5%, it is effectively impermeable to fluid flow. However, for brine volume fractions above 5%, the brine phase becomes macroscopically connected so that fluid pathways enable flow through the porous microstructure of the ice. For a typical bulk sea ice salinity of 5 parts per thousand, the 5% volume fraction corresponds to a critical temperature of about  $-5^{\circ}\text{C}$ ; hence the term “rule of fives.” Similarly, even casual inspection of aerial photos shows that the melt pond phase of the sea ice surface undergoes a percolation transition where disconnected ponds evolve into much larger scale connected structures with complex boundaries [15]. Connectivity of melt ponds promotes further melting and break-up of floes, as well as horizontal transport of meltwater and drainage through large vertical brine channels, cracks, leads, and seal holes [11, 6].

Establishing that the brine phase in sea ice actually exhibits a percolation transition, attended by critical behavior of the vertical fluid permeability, was accomplished through the development of X-ray

computed tomography for sea ice, and subsequent mapping of the data onto random graphs of nodes and edges [20, 21]. The connectivity of these graphs was analyzed as a function of temperature and sample size, and found to display a percolation threshold in the vertical direction around the 5% critical value conjectured in [19]. Furthermore, the theory of fluid and electrical transport through lattice percolation models [16, 17] was used to predict the dependence of the vertical component of the fluid permeability of sea ice as a function of brine volume fraction [20].

Other types of network models have been used to quantitatively describe the behavior of fluid flow through the porous sea ice microstructure. For example, in the random pipe model, the diameters of the pipes (assigned to the edges in a square lattice) are chosen from lognormal probability distributions that describe the cross-sectional areas of the brine inclusions in sea ice [22]. The fluid permeability of the model is computed by using a random resistor network representation of the system and employing a fast multigrid method to find its effective conductivity. This approach has also been used to directly model the electrical conductivity

of sea ice [23], an important parameter in remote sensing of sea ice thickness, transport properties, and microstructural transitions [24, 25, 26, 27, 28, 29].

Here we begin to develop techniques for network modeling of melt ponds, their connectivity, and horizontal flow characteristics. Some of the groundwork for this type of modeling was laid in [15]. Images of melting Arctic sea ice collected during two Arctic expeditions – the 2005 Healy-Oden TRans Arctic EXpedition (HOTRAX) [30] and the 1998 Surface Heat Budget of the Arctic Ocean (SHEBA) expedition [4] – were analyzed for area-perimeter data on thousands of individual melt ponds. Algorithmic methods of distinguishing melt ponds from the ocean in leads between the sea ice floes were developed. This data was used to discover that pond fractal dimension transitions from 1 to 2 around a critical length scale of 100 square meters in area [15]. Pond complexity was found to increase rapidly through the transition as smaller ponds coalesce to form large connected regions, reaching a maximum for ponds larger than about 1000 square meters whose boundaries resemble space filling curves.

In earlier work on melt ponds and sea ice albedo, image processing has been used to measure the area fractions of melt ponds and leads from aerial and satellite images. In [4] these area fractions from June to October, using SHEBA images taken in 1998 [4], show how the area fraction of melt ponds increases as summer progresses, and starts decreasing again at the end of summer as new ice forms. A probability distribution for the size of melt ponds is also derived from the data, which depends on the progress of the melt season.

In the work reported here, the connectivity of these melt pond networks is determined using aerial images of Arctic sea ice from the HOTRAX database. We develop an algorithmic method of mapping a configuration of melt ponds onto a graph of nodes and edges. These configurations may be disconnected into individual components, or partially or completely connected across an image. The edges are assigned values which indicate the width of the “bottlenecks” separating larger pools of melt water, which are identified with the nodes of the graph.

The volume of water in a melt pond results from the net balance of melt water accumulation, water in-flux from and

out-flux to neighboring ponds, drainage due to ice porosity, fluid permeability, and larger cracks in the pack ice. Some melt ponds may have large sink holes with high drainage rate. The flow of water between melt ponds depends on the narrowest bottlenecks between them and the width of these bottlenecks is inversely proportional to the fluid conductance between them. A conductance graph of the melt pond networks can help model the evolution of the melt pond configurations. Mathematical morphology based image processing techniques [31] are used with a clustering algorithm and graph theory to find a conductance graph associated with each melt pond configuration studied. Further work will explore the relationship of these graphs and associated conductance networks with the actual flow of fluid in the pond network, and the effect on sea ice albedo.

## 2. Method

The images provided by the SHEBA and HOTRAX expeditions are in color. The intensity and color of each pixel in the image is encoded using the intensities of the Red, Green and Blue colors that make up the pixel. The image is a matrix of pix-

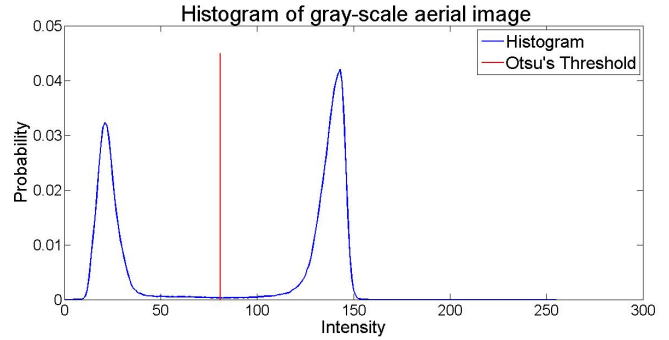
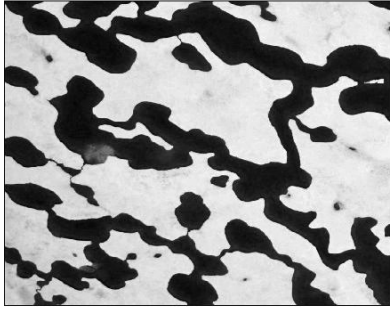


Figure 1: An aerial image of melt ponds from HOTRAX is shown on the left. A histogram of the image is shown on the right

els, with each pixel being a vector of three  
 230 variables - red, green and blue color values.  
 These are respectively called the red, green  
 and blue channels of the image.

These images are converted to gray-scale  
 because it reduces each pixel to only one  
 235 intensity and hence fewer computations are  
 required. This is done by using only the red  
 channel as it shows the most clear cut dif- 255  
 ference between ice and water intensities. A  
 simple thresholding operation is sufficient to  
 240 segment the melt pond water from ice and  
 get a binary image. Otsu's method [31] is  
 used to determine this threshold individu- 260  
 ally for each image, which is then segmented  
 based on this threshold. Figure 1 shows a  
 245 histogram of the intensity levels of a gray-  
 scale aerial image with Otsu's threshold.

The images used are cropped from those  
 in the SHEBA and HOTRAX databases,  
 which have dimensions around  $865 \times 770$   
 pixels. The size of the images does not af-  
 fect the algorithm as long as the resolution,  
 i.e., the number of pixels per unit physical  
 area covered, remains the same. Only the  
 processing time varies with image size.

### 2.1. Preprocessing the image

The binary image produced by Otsu's  
 method has small pieces of ice floating in  
 the melt ponds, melt ponds that are too  
 small to provide much information, and  
 other small artifacts due to noise. These  
 can clutter up the final connectivity graph  
 with unnecessary data. Basic mathemati-  
 cal morphology operations involving erosion  
 and dilation, as described in [31] are used to



265 clean up the image. A predetermined mask  
 or structuring element of fixed size is cen- 295  
 tered at each pixel of the image and only  
 those pixels, at which the structuring ele-  
 ment fits inside the original image, are set  
 270 to one. So, if a  $3 \times 3$  structuring element is  
 used, it will remove the outermost layer of 300  
 pixels from the foreground, a  $5 \times 5$  structur-  
 ing element would remove two layers and so  
 on. Morphological dilation is a complemen-  
 275 tary process where all those pixels, at which  
 the intersection between the structuring el-  
 ement and the image is non-zero, are set as 305  
 one. Dilation by a  $3 \times 3$  structuring element  
 would cause the foreground to grow another  
 280 layer of pixels. Opening involves erosion fol-  
 lowed by dilation with the same structuring  
 element and is used to remove smaller struc- 310  
 tures from the foreground like protrusions,  
 narrow connections, etc. Closing on the  
 285 other hand is dilation followed by erosion  
 and it fills in small gaps in the foreground.  
 Geodesic opening or closing involves finding 315  
 the intersection of the result of opening or  
 closing with the original image to preserve  
 290 the shape of the image. The image is first  
 cleaned up using geodesic opening of melt  
 ponds to remove inconsequential melt ponds 320  
 and geodesic closing to remove floating ice.

Circular masks are used for these processes  
 to maintain the curvy shapes of ponds. The  
 mask size can be adjusted as desired. Here  
 a  $3 \times 3$  mask is used. Note that care should  
 be taken to ensure that the mask size is at  
 least smaller than the narrowest bottleneck  
 in the image, otherwise this connection will  
 be lost.

## 2.2. Isolating melt ponds

The next step is to find individual melt  
 ponds. The previous step results in large  
 interconnected melt pond networks. First,  
 connected components are used to find all  
 the separate unconnected melt pond net-  
 works and label them. Each of these net-  
 works is then eroded progressively with a  
 3  $3 \times 3$  circular mask. At each erosion, some  
 ponds might break away from the main net-  
 work. These can be identified from an in-  
 crease in the number of unconnected re-  
 gions in the image, which are found us-  
 ing connected components. The connection  
 strength of the separated melt pond, to the  
 full network is proportional to the number  
 of iterations at which it breaks away. If a  
 region is split into multiple regions, the sep-  
 arated regions will form smaller networks  
 of melt ponds, which will all be connected

to each other. This step is repeated until 350 a pre-defined maximum bottleneck size is reached.

325 Also, a minimum pond size is set and if a region reaches this size, it is no longer split into smaller regions. This minimum pond 355 size is increased with increasing erosion iterations. The minimum pond size is scaled to maintain a minimum ratio  $\frac{\text{pond area}}{\text{bottleneck size}}$ . 330 This is done to avoid labeling connections between ponds as melt ponds themselves. An example of this is shown in Figure 2. 360

### 2.3. Connections between melt ponds

335 The last part of the problem is finding the conductances between the individual melt ponds. This is done in parallel as the inter- 365 connected melt ponds are being separated into smaller melt pond networks. Each erosion with a  $3 \times 3$  mask removes the out- 340 ermost pixel layer (perimeter-wise). Thus two layers of pixels, one from each side of 370 the bottleneck, are removed. Hence at each step, when a region splits into multiple re- 345 gions, the conductance between these regions will be  $2 \times i$ . Here  $i$  is the iteration number. The problem also requires that we find only direct connections between ponds. This means that if each pond is a node,

we must ignore connections that contain intermediate nodes in their paths. Consider the images in Figure 3. The interconnected pond splits into a number of smaller ponds in the same erosion step. The next step is to find out which ponds are directly connected to each other. Two simple methods of doing this would involve the following operations

1. morphological dilation,
2. a simple clustering approach followed by a graph theory method.

In the first method, at each iteration, the eroded image is subtracted from the original image to get only the bottlenecks that were eroded away. This resulting image is then dilated and a simple overlapping operation (using the logical OR function) is performed to check which ponds form a direct connection with each other. This is illustrated in Figure 4. A major problem with this approach is that sometimes the dilation is not sufficient to cause an overlap with the expected ponds and this leads to incorrect or missing connections.

In the second method, the center of each melt pond pixel-cluster is located using the mean of the cluster with Euclidean distances. One may try to use k-means clus-

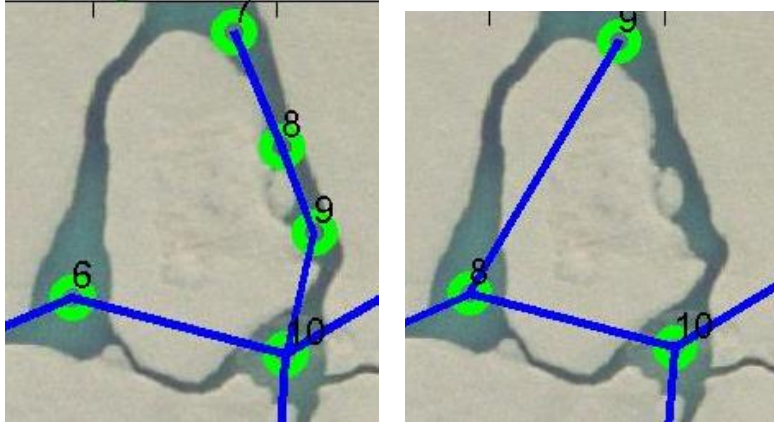


Figure 2: The connection between melt ponds is incorrectly labeled in the image on the left. Image on the right uses pond area scaling to correctly label melt ponds.

tering on the initial image to separate the ponds, but as this only uses euclidean distances between pixels and needs a fixed estimate of the number of clusters at the output, it will assign more than one cluster center to larger ponds and may ignore the smaller ponds. The geodesic distances between these cluster centers are calculated. The distance between unconnected ponds is considered to be an arbitrarily large number, which is larger than the maximum distance between two ponds. These distances are then used along with the conductance strengths calculated in section 2.2 to construct a graph of the melt pond network. Initially, the nodes of the graph are the cluster centers found above, and the all the

nodes belonging to connected melt ponds are connected to each other with edges. Note that the conductance strength here only refers to the width of the channel connecting different ponds and gives a basis for relative comparison of ease of flow of fluid between these channels. Let this conductance strength be denoted by  $\sigma_{ij}$  and the geodesic distance be  $d_{ij}$ . The weight of each edge is the ratio  $\frac{\sigma_{ij}}{d_{ij}}$ . Between two nodes, the direct path and all paths involving only one intermediate connection are considered. For any node, there are  $(n - 1)$  possible paths to another node, or  $(n - 2)$  indirect paths with one intermediate node and one direct path. The weight of the  $k$ th indirect path

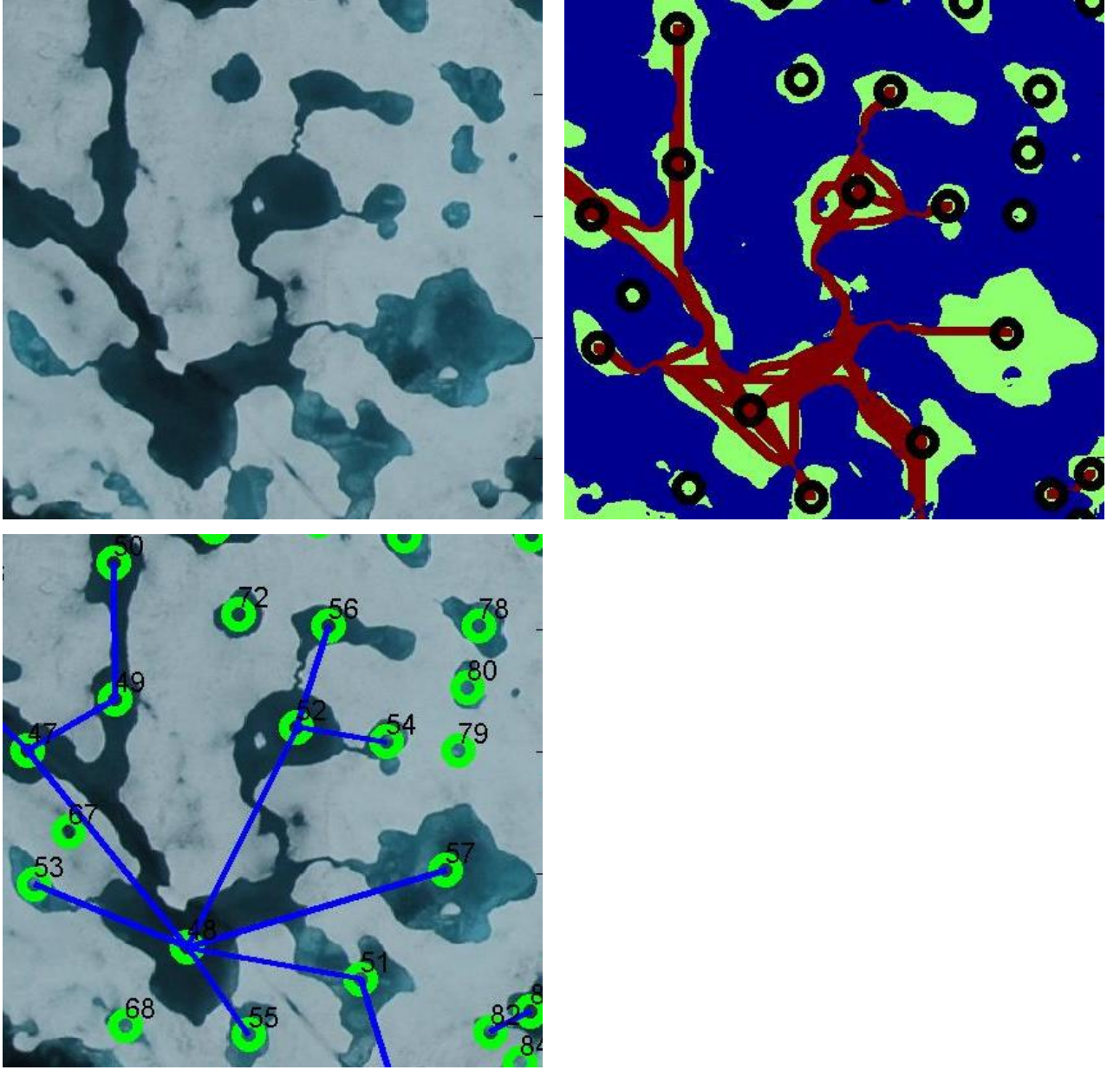


Figure 3: The figure on right at the top shows geodesic distances between melt pond nodes. The figure at the bottom shows the final connections obtained after edge elimination.

connecting two nodes is calculated as,

$$w_{ij}^{(k)} = \left( \frac{\sigma_{ik}}{d_{ik}} + \frac{\sigma_{kj}}{d_{kj}} \right), \quad \forall k \neq i, j. \quad (1)$$

Here  $\frac{\sigma_{ik}}{d_{ik}}$  is the weight of the edge from node  $i$  to node  $k$ . The weight of the edge which

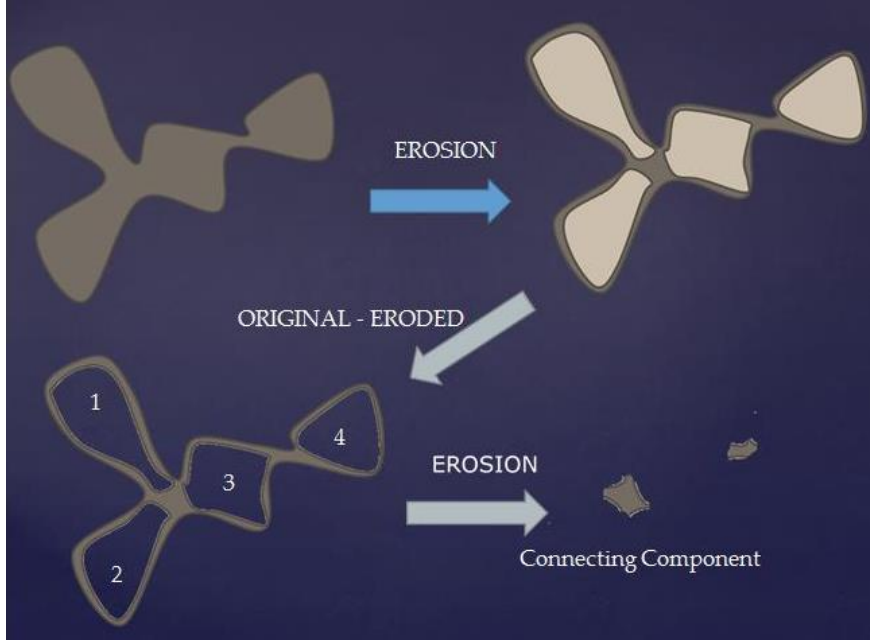


Figure 4: Mapping connections using morphological dilation.

directly connects nodes  $i$  and  $j$  is

$$w_{ij} = \frac{\sigma_{ij}}{d_{ij}}. \quad (2)$$

Only the path corresponding to the maximum weight between two nodes is retained and all the edges corresponding to other paths are dissolved. This favors paths which are either very short or have large conductances. At each step, one pair of nodes in the graph is considered. For the next pair, the previously updated connection graph is used so that the edges that no longer exist are not reconsidered. The final step of the algorithm is for node deletion, where the algorithm searches for very small nodes that

lie between two or more much larger nodes, and eliminates these small nodes based on a predetermined ratio. For the results presented later, this ratio is set to 20.

The latter graph method performs much better for mapping connections than the dilation method. Figure 5 shows the results obtained using the two different approaches. Consider the nodes 5 and 6 at the bottom right corner in the first figure. The connection between the two nodes is not detected because dilation of the connection shown in Figure 4 is not sufficient to overlap with ponds 5 and 6. Thus, pond 6 is shown connected directly to pond 1. This

issue is solved in the second figure by using the clustering and graph method.

#### 2.4. Conductivity factor calculations

To calculate the horizontal fluid “conductivity,” first two battery nodes are added to the left and right of the image. The left battery node is connected to all the ponds touching the left edge of the image with a conductance value of 1 for each connection. The right battery node is similarly connected. The purpose of the battery nodes is to simulate the computation of the effective or equivalent conductivity of a conductor network, which must be subjected to a potential difference, most easily visualized by connecting a battery. The conductivity across the network, between these battery nodes, is then measured. The conductivity of very large networks can be calculated approximately by considering smaller sections and then replacing these subsections with their equivalent conductivities. The conductivity of each section could be calculated to create a new, simpler graph model.

All the melt pond nodes which are not directly connected to a battery node in the graph are removed as they do not contribute to conductivity. To calculate the conductivity

between battery nodes, let  $c_{ij}$  be the conductivity of the edge between nodes  $i$  and  $j$ . Here, each  $c_{ij}$  is the normalized edge weight,  $w_{ij}$ , as described in the equation below.

$$c_{ij} = \frac{w_{ij}}{\max_{i,j}(w_{ij})} \forall i, j \quad (3)$$

Let the  $M$  be the total number of nodes in the graph, including the two battery nodes. We define the  $M \times M$  matrix  $A$  such that

$$A_{ij} = -c_{ij} \quad i, j = 1 \dots M, i \neq j \quad (4)$$

$$A_{ii} = \sum_{\forall j: j \neq i} c_{ij} \quad i = 1 \dots M \quad (5)$$

The matrix  $A'$  is the  $(M-1) \times (M-1)$  array obtained by removing the first row and column of  $A$ , which corresponds to the left battery node. Removing the last row and column of matrix  $A'$ , corresponding to right battery node, gives the  $(M-2)(M-2)$  matrix  $A''$ . The conductivity factor of the image represented by matrix  $A$ , between the battery nodes, is given by

$$\sigma(A) = \frac{\det(A')}{\det(A'')}. \quad (6)$$

It should be noted that the conductivity factor obtained is then related to the fluid permeability of the network, but not equal to the effective conductivity of the network, due to the length scale involved. As noted

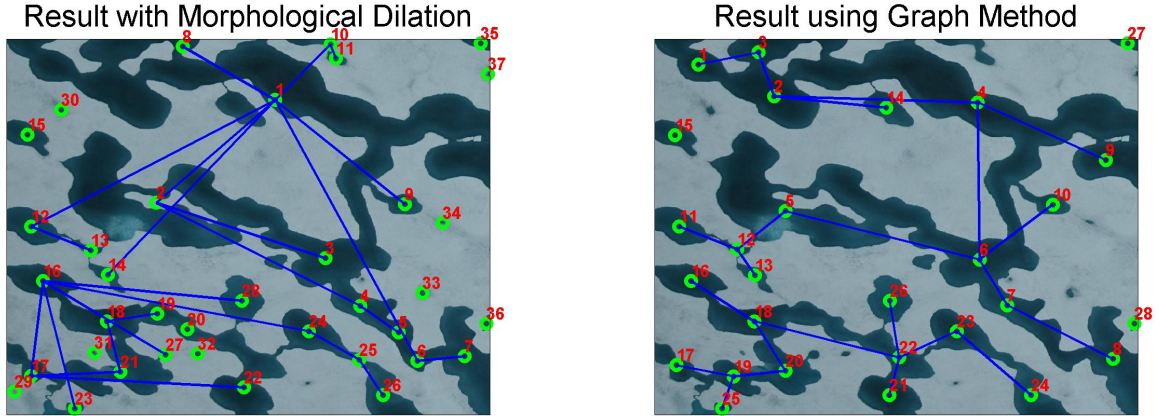


Figure 5: The image on the left results from using morphological dilation for mapping pond connections. The image on the right uses the clustering and graph method approach.

in the Introduction, further work will explore the relationship of this computed network conductivity to the horizontal fluid flow properties of melt pond configurations.

### 3. Results

The above method is used to generate the conductance graphs for different sets of images as described in Table 1. MATLAB is used to implement the method summarized above for each of these images.

This method was found to be most useful for images obtained in mid-summer, i.e. July, as the melt ponds are large and interconnected. The average time taken for different sets of images was calculated and is shown in table 2. The SHEBA images

taken in July were processed the quickest, because the images consist of larger and fewer melt ponds. Consequently, the operations involving connected components and the calculation of geodesic distances, do not occupy the processor for too long. When these times are compared to the August melt pond images from SHEBA, which have many more melt ponds per image, the computations take much longer. This can be easily rectified by selecting a smaller area of the image to give a faster and more accurate result. When images have a large number of melt ponds, the resolution of the calculated conductance values is reduced. Only about 10% of the computation time is spent in the calculation of geodesic distances and

Set	Month	Number	Database
1	June	5	SHEBA
2	July	10	SHEBA
3	August	10	HOTRAX

Table 1: List of images considered

using graph methods to eliminate all but the direct connections between melt ponds.

A major part of the computation time is spent in iteratively eroding the image, finding all the connected components and updating the bottleneck widths at each iteration. This can be sped up by using parallel processing for different connected components. Another step in reducing the time latency would be to ignore all ponds that have no other connections. However, this choice would be application specific, as even the isolated ponds may be used to study the evolution of networks with time.

Due to lack of any ground truth for these images, they are visually inspected to ascertain the performance of the method used. The processed images from July, August and June are shown in Figures 6, 7, 8, 9 and 10 respectively. Figure 11 shows the conductance graph obtained for the 3rd image in Figure 8. The conductivity factors

for these figures are shown in Tables 3, 4 and 5. The images shown in Figure 10 do not have any complete connections that go across the image from left to right. For this reason, the images are shown without removing nodes which are unconnected to the battery nodes. The conductivity factor values for all these images are zero.

## 4. Conclusion

After visual inspection, it can be concluded that the algorithm does a very good job of identifying melt ponds, labeling their connections and creating the conductance matrix. More work can be done to improve the speed of algorithm and remove the few mislabeling errors. The edge elimination method used assigns weights to the edges between nodes (melt pond centers) based on geodesic distance and widths of the connections. The function assigning weights to the edges can be modified and the weights



Set	Month	Database	Number of iterations	Average Time(minutes)
1	June	SHEBA	8	31.66
2	July	SHEBA	20	9.06
3	August	HOTRAX	20	18.04

Table 2: Average time to process each image

Image1	Image2	Image3	Image4	Image5
0	0	0	0	0

Table 3: Conductivities for image set 1

Image1	Image2	Image3	Image4	Image5
0	0	0	0	0
Image6	Image7	Image8	Image9	Image10
0	0.0546	0.0283	0.0443	0.2062

Table 4: Conductivities for image set 2

Image1	Image2	Image3	Image4	Image5
0	0.0542	0.1353	0.1216	0.0563
Image6	Image7	Image8	Image9	Image10
0.1778	0.1003	0.1078	0.0718	0.1127

Table 5: Conductivities for image set 3

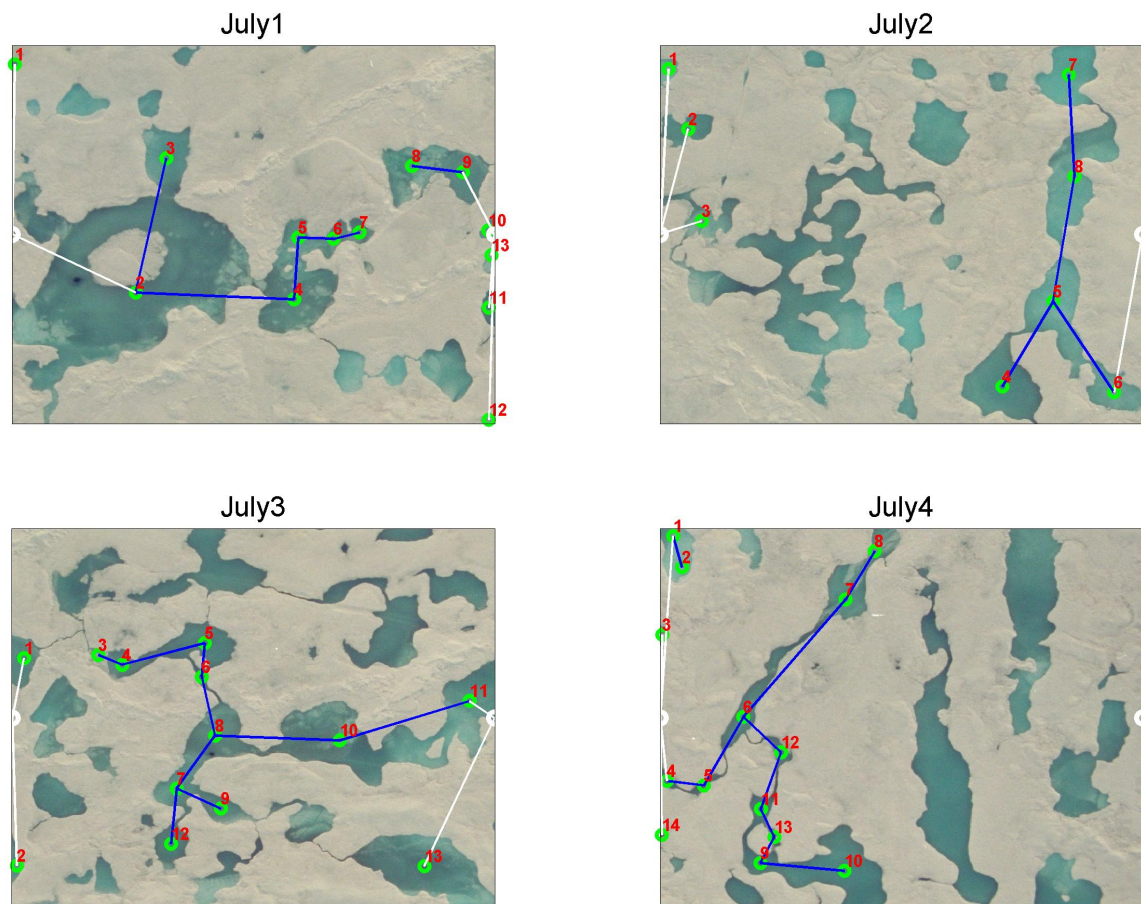


Figure 6: Melt ponds in July from SHEBA, continued on next page...

of the nodes (areas of melt ponds) can also be used in this function. 515

portant factor in climate models.

## Acknowledgments

The conductivity factors calculated can help to determine the rate at which melt water might drain from ponds to a sink node, which might be a sink hole in the ice pack. This water drainage influences ice pack albedo, and hence a calculation of the rate of drainage could prove to be an im-

We gratefully acknowledge support from the Division of Mathematical Sciences and the Division of Polar Programs at the U.S. National Science Foundation (NSF) through Grants DMS-1009704, ARC-0934721, DMS-0940249, and DMS-

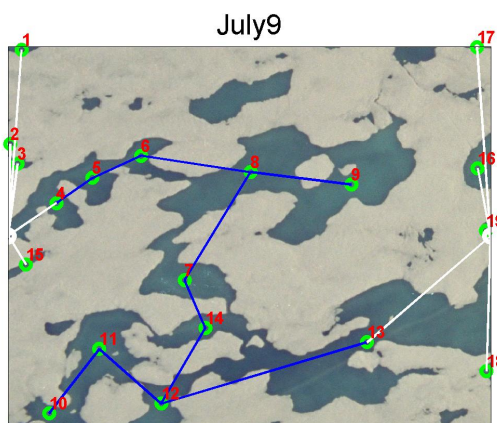
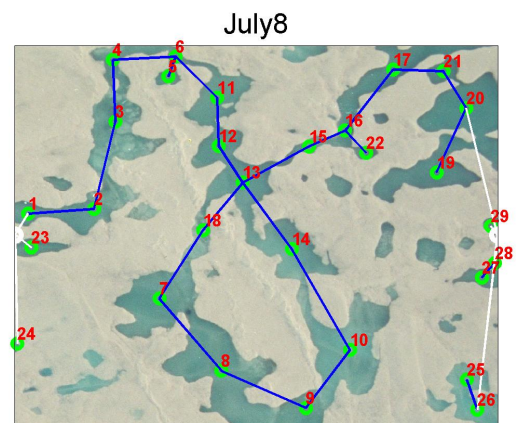
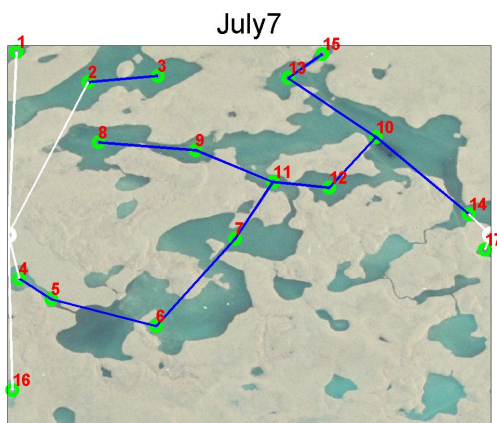
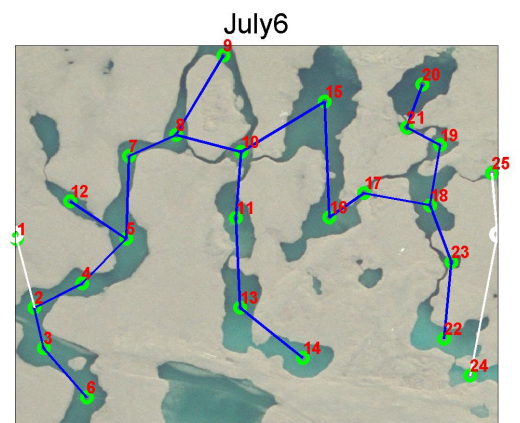
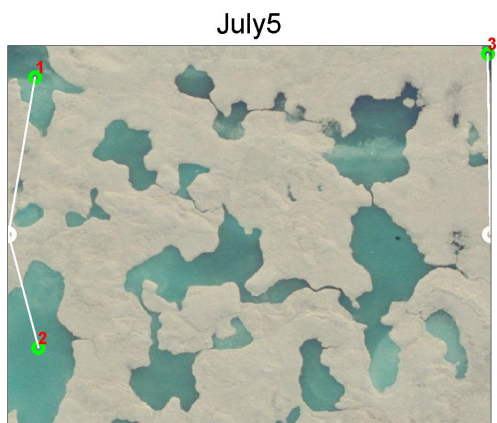


Figure 7: ...continued, Melt ponds in July from SHEBA



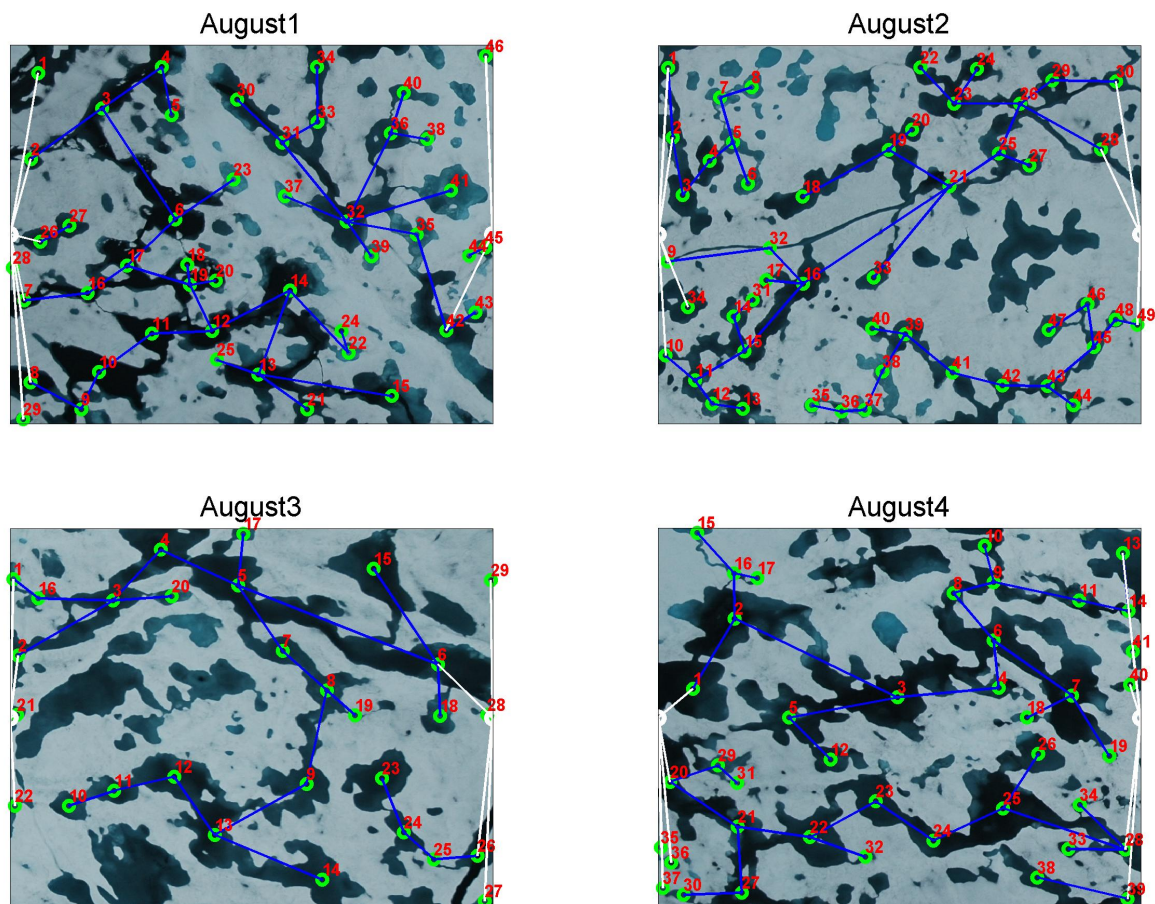


Figure 8: Melt ponds in August from HOTRAX, continued on next page...

1413454. We are also grateful for support  
 from the Office of Naval Research (ONR)  
 through Grant N00014-13-10291. We would  
 like to thank the NSF Math Climate Re-  
 search Network (MCRN) as well for their  
 support of this work, and Don Perovich for  
 providing the melt pond images.

## References

- [1] J. Stroeve, M. M. Holland, W. Meier, T. Scambos, M. Serreze, Arctic sea ice decline: Faster than forecast, *Geophys. Res. Lett.* 34 (9) (2007) L09591, doi: 10.1029/2007GL029703.
- [2] J. Boé, A. Hall, X. Qu, September sea-ice cover in the Arctic Ocean projected to vanish by 2100, *Nature Geoscience* 2 (doi: 10.1038/NGEO467) (2009) 341–343.
- [3] M. C. Serreze, M. M. Holland, J. Stroeve,

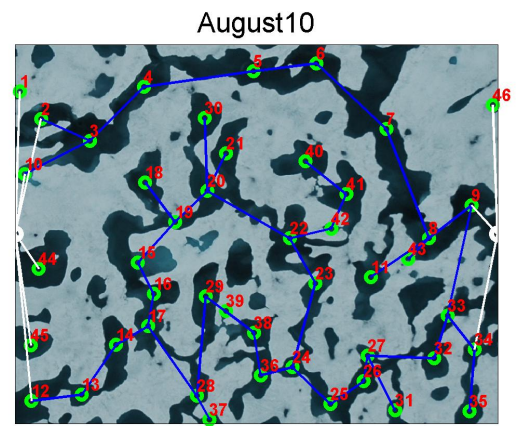
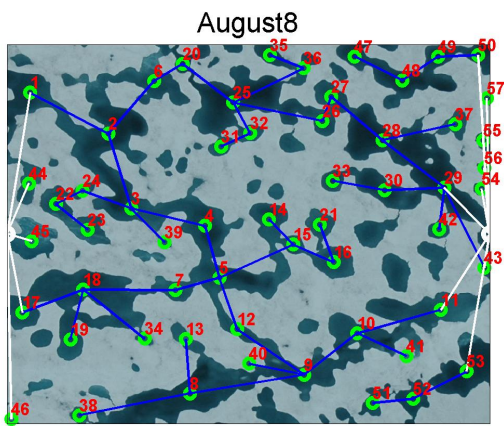
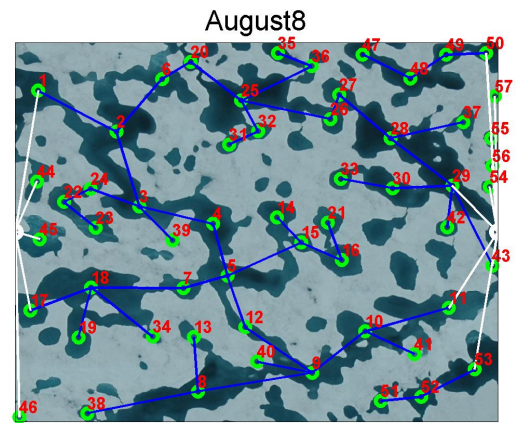
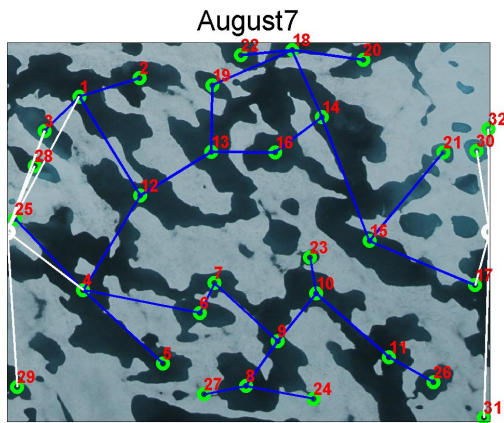
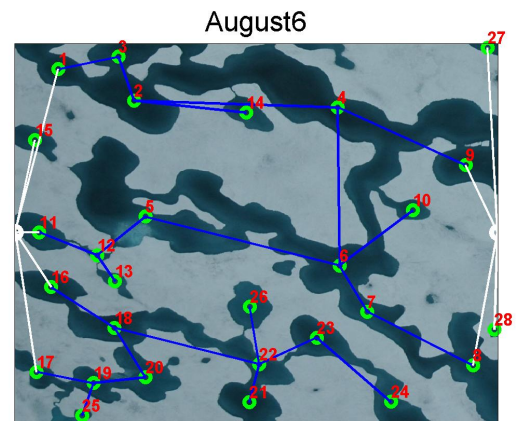
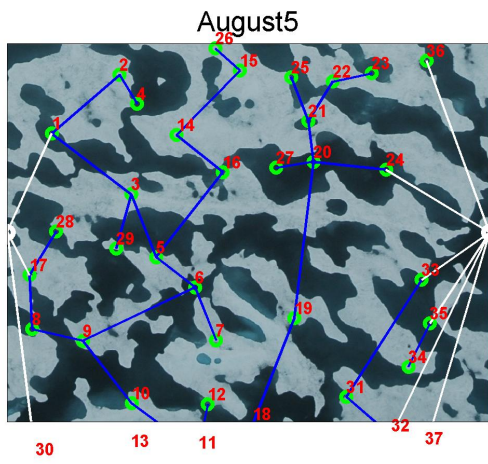


Figure 9: ...continued, Melt ponds in August from HOTRAX



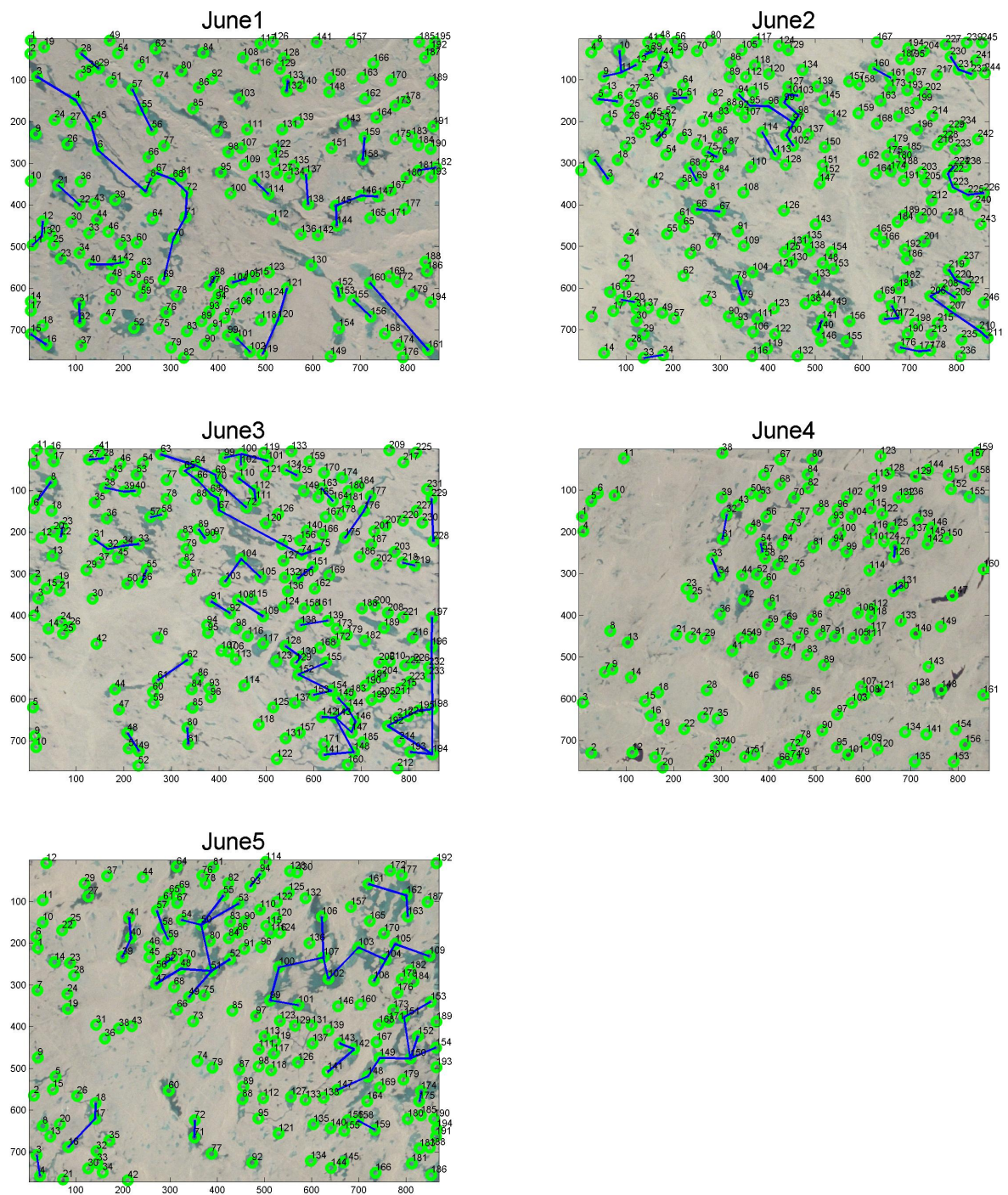


Figure 10: Melt ponds in June from SHEBA

	A	B	C	D	E	F	G	H	I	J	K	L	M	N	O	P	Q	R	S	T	U	V	W	X	Y	Z	AA	AB	AC	AD	AE
1	0	1	1	0	0	0	0	0	0	0	0	0	0	0	0	0	0	0	0	0	0	1	1	0	0	0	0	0	0	0	0
2	1	0	0	0	0	0	0	0	0	0	0	0	0	0	0	0	0.18	0	0	0	0	0	0	0	0	0	0	0	0	0	0
3	1	0	0	0.47	0	0	0	0	0	0	0	0	0	0	0	0	0	0	0	0	0	0	0	0	0	0	0	0	0	0	0
4	0	0	0.47	0	1	0	0	0	0	0	0	0	0	0	0	0	0.24	0	0	0	0.06	0	0	0	0	0	0	0	0	0	0
5	0	0	0	1	0	0.65	0	0	0	0	0	0	0	0	0	0	0	0	0	0	0	0	0	0	0	0	0	0	0	0	0
6	0	0	0	0	0.65	0	0.71	0.41	0	0	0	0	0	0	0	0	0	0.24	0	0	0	0	0	0	0	0	0	0	0	0	0
7	0	0	0	0	0	0.71	0	0	0	0	0	0	0	0	0	0.29	0	0	0.18	0	0	0	0	0	0	0	0	0	0	0	1
8	0	0	0	0	0	0.41	0	0	0.71	0	0	0	0	0	0	0	0	0	0	0	0	0	0	0	0	0	0	0	0	0	0
9	0	0	0	0	0	0	0	0.71	0	0.47	0	0	0	0	0	0	0	0	0	0.12	0	0	0	0	0	0	0	0	0	0	0
10	0	0	0	0	0	0	0	0	0.47	0	0	0	0	0.35	0	0	0	0	0	0	0	0	0	0	0	0	0	0	0	0	0
11	0	0	0	0	0	0	0	0	0	0	0	0.35	0	0	0	0	0	0	0	0	0	0	0	0	0	0	0	0	0	0	0
12	0	0	0	0	0	0	0	0	0	0	0.35	0	0.76	0	0	0	0	0	0	0	0	0	0	0	0	0	0	0	0	0	0
13	0	0	0	0	0	0	0	0	0	0	0	0.76	0	0.76	0	0	0	0	0	0	0	0	0	0	0	0	0	0	0	0	0
14	0	0	0	0	0	0	0	0	0	0.35	0	0	0.76	0	0.71	0	0	0	0	0	0	0	0	0	0	0	0	0	0	0	0
15	0	0	0	0	0	0	0	0	0	0	0	0	0	0.71	0	0	0	0	0	0	0	0	0	0	0	0	0	0	0	0	0
16	0	0	0	0	0	0.29	0	0	0	0	0	0	0	0	0	0	0	0	0	0	0	0	0	0	0	0	0	0	0	0	0
17	0	0.18	0	0.24	0	0	0	0	0	0	0	0	0	0	0	0	0	0	0	0	0	0	0	0	0	0	0	0	0	0	0
18	0	0	0	0	0	0.24	0	0	0	0	0	0	0	0	0	0	0	0	0	0	0	0	0	0	0	0	0	0	0	0	0
19	0	0	0	0	0	0	0.18	0	0	0	0	0	0	0	0	0	0	0	0	0	0	0	0	0	0	0	0	0	0	0	0
20	0	0	0	0	0	0	0	0	0.12	0	0	0	0	0	0	0	0	0	0	0	0	0	0	0	0	0	0	0	0	0	0
21	0	0	0	0.06	0	0	0	0	0	0	0	0	0	0	0	0	0	0	0	0	0	0	0	0	0	0	0	0	0	0	0
22	1	0	0	0	0	0	0	0	0	0	0	0	0	0	0	0	0	0	0	0	0	0	0	0	0	0	0	0	0	0	0
23	1	0	0	0	0	0	0	0	0	0	0	0	0	0	0	0	0	0	0	0	0	0	0	0	0	0	0	0	0	0	0
24	0	0	0	0	0	0	0	0	0	0	0	0	0	0	0	0	0	0	0	0	0	0	0	0	0.06	0	0	0	0	0	0
25	0	0	0	0	0	0	0	0	0	0	0	0	0	0	0	0	0	0	0	0	0	0	0	0.06	0	0.12	0	0	0	0	0
26	0	0	0	0	0	0	0	0	0	0	0	0	0	0	0	0	0	0	0	0	0	0	0	0	0	0.12	0	0.12	0	0	0
27	0	0	0	0	0	0	0	0	0	0	0	0	0	0	0	0	0	0	0	0	0	0	0	0	0	0.12	0	0	0	0	1
28	0	0	0	0	0	0	0	0	0	0	0	0	0	0	0	0	0	0	0	0	0	0	0	0	0	0	0	0	0	0	1
29	0	0	0	0	0	0	0	0	0	0	0	0	0	0	0	0	0	0	0	0	0	0	0	0	0	0	0	0	0	0	1
30	0	0	0	0	0	0	0	0	0	0	0	0	0	0	0	0	0	0	0	0	0	0	0	0	0	0	0	0	0	0	1
31	0	0	0	0	0	0	1	0	0	0	0	0	0	0	0	0	0	0	0	0	0	0	0	0	0	0	1	1	1	1	0

Figure 11: Conductance values for August (HOTRAX 3rd photograph)

- Perspectives on the Arctic's shrinking sea-ice cover, *Science* 315 (2007) 1533–1536.
- [4] D. K. Perovich, W. B. T. III, K. Ligett, Aerial observations of the evolution of ice surface conditions during summer, *J. Geophys. Res.* 107 (C10) (2002) doi:10.1029/2000JC000449.
- [5] F. Scott, D. L. Feltham, A model of the three-dimensional evolution of Arctic melt ponds on first-year and multiyear sea ice, *J. Geophys. Res.* 115 (2010) C12064, doi:10.1029/2010JC006156.
- [6] C. Polashenski, D. Perovich, Z. Courville, The mechanisms of sea ice melt pond formation and evolution, *J. Geophys. Res.* C (Oceans) 117 (2012) C01001 (23 pp.), doi:10.1029/2011JC007231.
- [7] J. A. Curry, J. L. Schramm, E. E. Ebert, On the sea ice albedo climate feedback mechanism, *J. Climate* 8 (1995) 240–247.
- [8] D. K. Perovich, J. A. Richter-Menge, K. F. Jones, B. Light, Sunlight, water, and ice: Extreme Arctic sea ice melt during the summer of 2007, *Geophys. Res. Lett.* 35 (2008) L11501, doi:10.1029/2008GL034007.
- [9] D. Flocco, D. L. Feltham, A. K. Turner, Incorporation of a physically based melt pond scheme into the sea ice component of a climate model, *J. Geophys. Res.* 115 (2010) C08012 (14 pp.), doi:10.1029/2009JC005568.
- [10] C. A. Pedersen, E. Roeckner, M. L  thje, J. Winther, A new sea ice albedo scheme including melt ponds for ECHAM5 general circulation model, *J. Geophys. Res.* 114 (2009) D08101, doi:10.1029/2008JD010440.

- [11] R. K. Scharien, J. J. Yackel, Analysis of surface roughness and morphology of first-year sea ice melt ponds: Implications for microwave scattering, *IEEE Trans. Geosci. Rem. Sens.* 43 (2005) 2927.
- [12] D. Flocco, D. L. Feltham, A continuum model of melt pond evolution on Arctic sea ice, *J. Geophys. Res.* 112 (2007) C08016, doi:10.1029/2006JC003836.
- [13] E. D. Skyllingstad, C. A. Paulson, D. K. Perovich, Simulation of melt pond evolution on level ice, *J. Geophys. Res.* 114 (2009) C12019, doi:10.1029/2009JC005363.
- [14] E. C. Hunke, W. H. Lipscomb, CICE: the Los Alamos Sea Ice Model Documentation and Software Users Manual Version 4.1 LA-CC-06-012, t-3 Fluid Dynamics Group, Los Alamos National Laboratory (2010).
- [15] C. Hohenegger, B. Alali, K. R. Steffen, D. K. Perovich, K. M. Golden, Transition in the fractal geometry of Arctic melt ponds, *The Cryosphere* 6 (2012) 1157–1162.
- [16] D. Stauffer, A. Aharony, Introduction to Percolation Theory, Second Edition, Taylor and Francis Ltd., London, 1992.
- [17] K. Christensen, N. R. Moloney, Complexity and Criticality, Imperial College Press, London, 2005.
- [18] S. R. Broadbent, J. M. Hammersley, Percolation processes I. Crystals and mazes 53 (1957) 629–641.
- [19] K. M. Golden, S. F. Ackley, V. I. Lytle, The percolation phase transition in sea ice, *Science* 282 (1998) 2238–2241.
- [20] K. M. Golden, H. Eicken, A. L. Heaton, J. Miner, D. Pringle, J. Zhu, Thermal evolution of permeability and microstructure in sea ice, *Geophys. Res. Lett.* 34 (2007) L16501 (6 pages and issue cover), doi:10.1029/2007GL030447.
- [21] D. J. Pringle, J. E. Miner, H. Eicken, K. M. Golden, Pore-space percolation in sea ice single crystals, *J. Geophys. Res. (Oceans)* 114 (2009) C12017, 12 pp., doi:10.1029/2008JC005145.
- [22] J. Zhu, A. Jabini, K. M. Golden, H. Eicken, M. Morris, A network model for fluid transport in sea ice, *Ann. Glaciol.* 44 (2006) 129–133.
- [23] J. Zhu, K. M. Golden, A. Gully, C. Sampson, A network model for electrical transport in sea ice, *Physica B (Condensed Matter)* 405 (14-15) (2010) 3033–3036.
- [24] K. Fujino, Y. Suzuki, An attempt to estimate the thickness of sea ice by electrical resistivity method ii, *Low Temp. Sci.* A21 (1963) 151–157.
- [25] J. Addison, Electrical properties of saline ice 40 (1969) 3105–3114.
- [26] F. Thyssen, H. Kohnen, M. V. Cowan, G. W. Timco, DC resistivity measurements on the sea ice near pond inlet, *Polarforschung* 44 (1974) 117–126.
- [27] R. G. Buckley, M. P. Staines, W. H. Robinson, In situ measurements of the resistivity of Antarctic sea ice, *Cold Reg. Sci. Technol.* 12 (3) (1986) 285–290.
- [28] J. E. Reid, A. Pfaffling, A. P. Worby, J. R. Bishop, In situ measurements of the direct-



current conductivity of Antarctic sea ice: Implications for airborne electromagnetic sounding of sea-ice thickness, *Ann. Glaciol.* 44 (2006) 217–223.

[29] M. Ingham, D. J. Pringle, H. Eicken, Cross-borehole resistivity tomography of sea ice, *Cold Reg. Sci. Technol.* 52 (2008) 263–277, 10.1016/j.coldregions.2007.05.002.

[30] D. K. Perovich, T. C. Grenfell, B. Light, B. C. Elder, J. Harbeck, C. Polashenski, W. B. T. III, C. Stelmach, Transpolar observations of the morphological properties of Arctic sea ice, *J. Geophys. Res.* 114 (2009) C00A04, doi:10.1029/2008JC004892.

[31] R. C. Gonzalez, R. E. Woods, Digital image processing, Prentice Hall Third Edition.